



Sorption mechanism of lead ions onto manganese oxide-modified diatomite from aqueous solutions

Lili Ma^a, Qinglin Xie^{b,*}, Nanchun Chen^c, Hui Xu^b, Qingfeng Yu^d, Haimiao Zhou^a

^aCollege of Environmental Science and Engineering, Guilin University of Technology, Guilin, Guangxi Zhuang Autonomous Region, China, 541004, Tel. +86 13217733210, email: 2006025@glut.edu.cn (L. Ma), Tel. +86 18100761300, email: 383467704@qq.com (H. Zhou)

^bCollaborative Innovation Center for Water Pollution Control and Water Safety in Karst Area, Guilin University of Technology, Guilin, Guangxi Zhuang Autonomous Region, China, 541004, Tel. +86 13667736699, email: xqinglin@hotmail.com (Q. Xie), Tel. +86 15677338046, email: 791550400@qq.com (H. Xu)

^cKey Laboratory of Nonferrous Material and Advanced Processing Technology of Ministry of Education, Guilin University of Technology, Guilin, Guangxi Zhuang Autonomous Region, China, 541004, Tel. +86 18978368382, email: cnc@glut.edu.cn (N. Chen)

^dGuangxi Key Laboratory of Environmental Pollution Control Theory and Technology, Guilin University of Technology, Guilin, Guangxi Zhuang Autonomous Region, China, 541004, Tel. +86 13737725835, email: 719136817@qq.com (Q. Yu)

Received 1 December 2017; Accepted 2 September 2018

ABSTRACT

In this work, manganese oxide was used to coat the surface of diatomite, forming a novel modified adsorbent (referred to as Mn-diatomite). Because the structural changes that occurred during the modification and adsorption processes are critical to formulating effective adsorption system designs, various analytical techniques were used to characterize the Mn-diatomite structure and its adsorbent mechanisms, including scanning electron microscopy (SEM), Fourier transform infrared spectroscopy (FTIR), X-ray diffraction (XRD), and atomic absorption spectrometry (AA). The results showed that the active hydroxyl on the diatomite surface disappeared after modification, and Mn-O-Si groups were newly generated, suggesting that MnO₂ was successfully grafted onto the surface of diatomite after modification. The feasibility of using Mn-diatomite as an adsorbent for removal of Pb(II) ions was explored using the batch equilibrium technique with various controlled experimental parameters, such as adsorbent dose, pH, and initial Pb(II) concentration. Further analysis showed that the removal process followed the Langmuir isotherms and pseudo-second-order kinetics models. Reusability studies indicated that the lead adsorption capacity did not change remarkably after ten sorption-desorption cycles. These cumulative results suggested that Mn-diatomite can be used as an adsorbent for efficient removal of Pb(II) from aqueous solutions.

Keywords: Diatomite; Manganese oxides; Pb(II); Adsorption; Kinetic

1. Introduction

Heavy metals are toxic substances, and they are generated as byproducts from metallurgical industries, electroplating, battery manufacturing, landfill leachates, and other sources. Heavy metals discharged into the environment are persistent; they can change form, be transferred, and become diluted or bioaccumulated, but they cannot be degraded. Lead is one of the most widespread and lethal heavy metals, which may cause anemia, brain

damage, anorexia, encephalopathy, irritability, malaise, and various symptoms related to the nervous system [1]. Lead and its compounds can endanger human health, even at low concentration ratios in water, by accumulating in animals and plants and being transported through food chains. Therefore, the removal of lead from wastewater is very important with respect to the environment and public health.

Several physico chemical methods have been used to remove lead from aqueous solutions, including chemical coagulation, ion exchange, adsorption, extraction, and membrane separation processes [2]. Among these methods,

*Corresponding author.

adsorption is highly popular because of its simplicity, moderate operational conditions, and economic feasibility, and hence adsorption has been widely applied in heavy metal wastewater treatment processes [3]. Identifying an adsorbent that is economical, environmentally friendly, and has a high adsorption capacity is important to further enhance adsorption methods.

Diatomite is a fine grained, low-density biogenic sediment that consists essentially of amorphous silica ($\text{SiO}_2 \cdot n\text{H}_2\text{O}$) derived from the opalescent frustules of fossilized diatoms. Although natural diatomite has a low adsorption capacity [4], diatomite can react with many polar functional groups because of the presence of silanol groups that spread over the silica matrix [5]. Al-Ghouti showed that diatomite impregnated with manganese oxides was an effective adsorbent for removing heavy metals from aqueous solutions [6]. Manganese oxides are regarded as good scavengers of heavy metal ions [7].

In this study, manganese oxides were used to modify diatomite, and the capacity of manganese oxide-modified diatomite (Mn-diatomite) to adsorb Pb(II) was investigated. Determining the structural changes that occur during adsorbent modification and adsorption mechanisms are essential for effective adsorption system designs [7]. Therefore, this study applied various analytical techniques to characterize the structure of Mn-diatomite and mechanisms of the modification and Pb adsorption processes, including scanning electron microscopy (SEM), Fourier transform infrared spectroscopy (FTIR), X-ray diffraction (XRD), and atomic absorption spectrometry (AA).

2. Materials and methods

2.1. Materials

Diatomite samples used in this experiment were collected from Sichuan, China. X-ray fluorescence analysis of the diatomite revealed that the diatomite consisted mainly of SiO_2 (81.81%), as well as 6.99% Al_2O_3 , 1.58% Fe_2O_3 , 0.57% CaO , 1.54% MgO , 1.219% K_2O , 0.856% Na_2O , 0.295% TiO_2 , 0.052% P_2O_5 , 0.018% MnO , and 4.37% loss on ignition.

The $\text{Pb}(\text{NO}_3)_2$, MnCl_2 , NaOH , and HCl used in this study were analytical grade reagents obtained from Guangzhou Chemical Reagent Co. (Guangzhou, China). All other reagents and solvents used were also analytical grade without further purification, and distilled water was used in the preparation of all solutions.

2.2. Preparation of Mn-diatomite sorbent

The procedures for the chemical modification were as follows: 15 g of diatomite were mixed with 50 mL of 4 mol/L NaOH at 90°C for 2 h. Subsequently, 100 mL of 2 mol/L MnCl_2 was added to the mixture, while the pH was maintained between 1 and 2 with HCl . The mixture was stirred continuously for 24 h at room temperature. To increase the formation rate of $\text{Mn}(\text{OH})_2$, the diatomite was re-mixed with 25 mL of 2 mol/L MnCl_2 at room temperature for 24 h. The excess was decanted and the diatomite was left exposed to air to facilitate oxidation of the $\text{Mn}(\text{OH})_2$. The sample was then washed with distilled water, dried in an oven at 105°C,

and pounded in a porcelain mortar to form a powdered mixture. The powder was then placed into polyethylene bags labeled "Mn-diatomite" and stored for future use.

2.3. Characterization tests

The morphology of the Mn-diatomite was determined by SEM (JSM-6380LV). Vibrations of the sample skeletons were analyzed by FTIR (NEXUS 470, USA) using KBr pellets; the scanning wavenumber ranged between 400 and 4000 cm^{-1} . Chemical valence states of samples were analyzed by X-ray photoelectron spectrometer (XPS, ESCALAB 250Xi) with a monochromatized AlK_α (1486.6 eV) ray as the excitation light source. All tested samples were calibrated by C_{1s} (284.8 eV) standard pollution peaks. Sample phases were analyzed by X-ray diffraction (XRD, X'Pert PRO). The specific surface area and the pore size distribution were determined using a specific surface area analyzer (ASAP 2020 HD88).

2.4. Adsorption tests

The batch adsorption experiments for the removal of Pb(II) were examined at different adsorbent doses, pH values, and initial metal ion concentrations. The adsorbent was placed into 250-mL Erlenmeyer flasks, and then 100 mL of Pb(II) solution was added. Each flask was placed in an SHZ-82 gyratory thermostatic water bath shaker at 200 r/min until the adsorption equilibrium was attained. The mass fraction of Pb(II) in water samples after adsorption were tested by a PE-AA 700 atomic absorption spectrometer. The test results were used to calculate the removal rate and adsorption capacity according to Eqns. (1) and (2):

Removal rate

$$\eta = (1 - C_e/C_0) \times 100\% \quad (1)$$

Adsorption capacity

$$q = (C_0 - C_e)V/M \quad (2)$$

where C_0 is the initial concentration of the Pb(II) ion solution, C_e is the concentration of Pb(II) ion present at equilibrium (mg/L), V is the volume of the solution (L), and M is the mass of adsorbent employed (g).

3. Results and discussion

In order to elucidate the adsorption mechanisms, a variety of analytical techniques were employed, including SEM, FTIR, XRD, and XPS, and the results are discussed in the following subsections.

3.1. Characterization of diatomite

3.1.1. Morphological analysis of diatomite

SEM images of diatomite and Mn-diatomite are shown in Fig. 1, where (a1) and (a2) show diatomite samples and

(b1) and (b2) show Mn-diatomite samples. Most diatoms were disc sieve-shaped with many micro pores on the surface. The Mn-diatomite samples maintained the original diatomite shape and spatial structure but were covered by the modifying substance. The modifier was interfaced to the diatomite surface very well.

3.1.2. Specific surface area and pore diameter analysis

The pore volume changes in relation to the pore diameter of diatomite and Mn-diatomite are shown in Fig. 2. The pore diameters were mostly the range between 4 and 10 nm before and after modification; this range belongs to the meso porous range (between 2 and 50 nm) [3,4]. The pore diameter changed a little after modification, and the uniformity of the size distribution clearly improved, which was due to the removal of impurities from the diatomite pores.

The specific surface areas and pore diameters of diatomite and modified diatomite are shown in Table 1. The diatomite had a high specific surface area, and the specific surface area of Mn-diatomite was almost eight times that of diatomite. This result is especially significant because high specific surface areas benefit heavy metal adsorption. The pore diameter changed only 0.26 nm after modification.

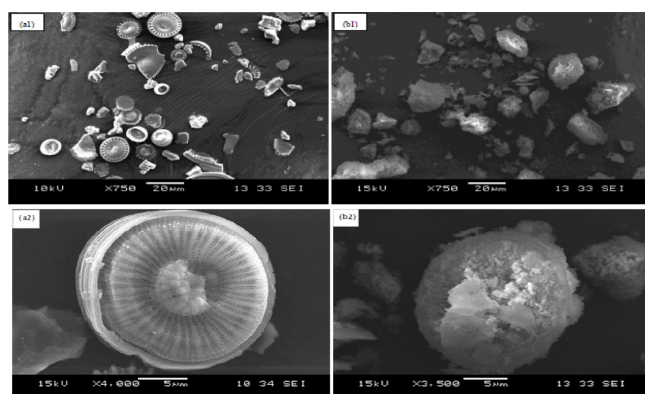


Fig. 1. SEM images of diatomite (a) and Mn-diatomite (b).

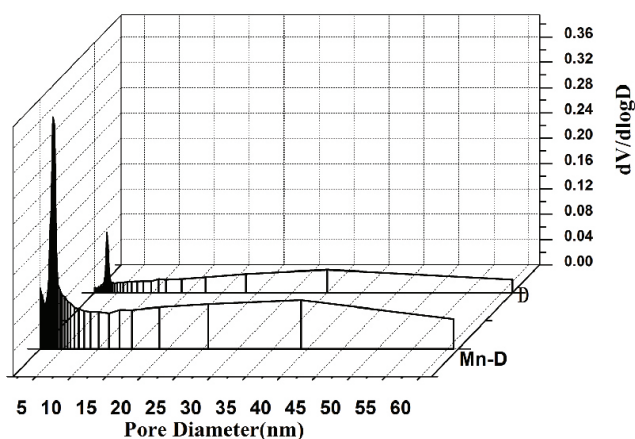


Fig. 2. Pore volume changes in relation to pore diameter of diatomite (D) and Mn-diatomite (Mn-D).

Table 1

Specific surface area and pore diameter of diatomite and Mn-diatomite

	Diatomite	Mn-diatomite
Specific surface area (m ² /g)	19.302	148.253
Pore diameter (nm)	7.498	7.758

3.1.3. FTIR analysis

FTIR analysis was performed from 400 to 4000 cm⁻¹ to investigate the surface characteristics of the diatomite and Mn-diatomite. FTIR spectra of the diatomite, Mn-diatomite, and Mn-diatomite after Pb adsorption were expected to yield important information about these materials' chemical structures. A peak observed at 467 cm⁻¹ was due to the antisymmetric bending vibration of O–Si–O; that at 694 cm⁻¹ was due to the symmetric stretching vibration of Si–O–Si; that at 1095 cm⁻¹ was due to the antisymmetric stretching vibration of Si–O [8,9]; all of the above peaks from the Mn-diatomite before and after Pb adsorption were weaker than those of unmodified diatomite. The peak at 796 cm⁻¹ was due to the symmetric stretching vibration of Si–O, the intensity of which decreased and shifted to low wave numbers after MnO modification, and the peak intensity weakened further after Pb adsorption, which was in good agreement with the XRD results. The weak and narrow bands at 3695 and 3619 cm⁻¹ were due to free surface silanol (Si–OH) [5]. After modification, the band intensities at 3695 and 3619 cm⁻¹ almost disappeared because of the chemical interactions between the oxides and the surface silanol groups. The strong and broad band at 3431 cm⁻¹ was due to the antisymmetric stretching vibration of free water hydroxyl (–OH) [10]. The bands at 1382 and 1633 cm⁻¹ were due to the bending vibration of free water H–O–H. The bands at 2852 and 2922 cm⁻¹ were due to hydroxyl-associated hydrogen bonds, which disappeared after adsorption. The most important peak present in the FTIR spectrum of Mn-diatomite occurred at 528 cm⁻¹, which corresponds to the Mn–O stretching vibration [11]. From the spectral analysis, it is evident that MnO₂ was successfully deposited on the diatomite surface.

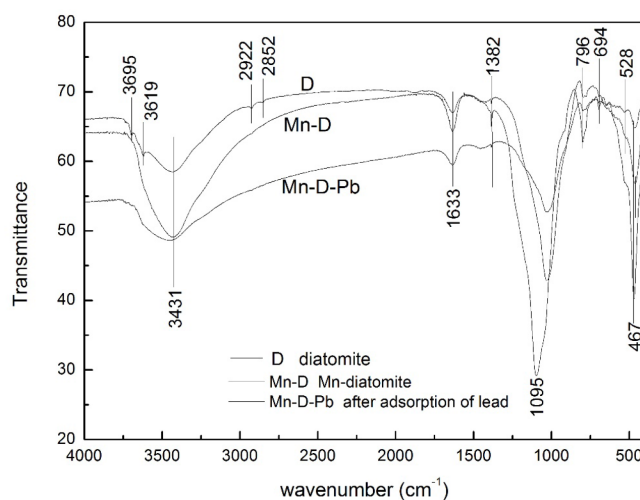


Fig. 3. FTIR spectra of diatomite (D), Mn-diatomite (Mn-D) and Mn-diatomite after Pb sorption (Mn-D-Pb).

3.1.4. XRD analysis

XRD spectra of diatomite (D) and Mn-diatomite (Mn-D) samples are shown in Fig. 4. The diatomite sample was mainly composed of natural amorphous SiO₂. There was a broad peak at 2θ = 18–32° on the XRD spectrum of the diatomite sample, which indicated that the diatomite had the amorphous [SiO₄] structure. In addition to the SiO₂ diffraction peak, the diatomite sample also contained peaks indicating AlSi material ("2" in Fig. 4) and organic phase ("3"). The low intensities of the diffraction peaks of cristobalite (2θ = 25.5–30.5°, "a") and montmorillonite (2θ = 15–20.5°, "b") indicated relatively low content.

In the XRD spectra of the Mn-diatomite sample, the broad peak disappeared and the intensity of the SiO₂ peak decreased. These results were thought to be due to the modifier grafted to the diatomite surface. Meanwhile, the organic diffraction peak at 2θ = 5–10° disappeared, which indicated that the organic material had been removed or destroyed. The intensities of the cristobalite peak ("a") and montmorillonite peak ("b") decreased, indicating decreased content during the modification process. The newly generated MnO₂ peak ("4") in the Mn-diatomite sample indicated that the modifier effectively grafted with the diatomite surface.

3.1.5. XPS analysis

Changes in the chemical state and molecular structure of the diatomite surface induced by the modification and adsorption processes were revealed by XPS analysis of the main elements O and Si of the diatomite matrix and the modifier Mn. The O1s XPS patterns of diatomite (D) and Mn-diatomite (Mn-D) are shown in Fig. 5. The O1s XPS pattern of Mn-diatomite was obviously asymmetric and shifted toward a low binding energy, which indicated that the binding energy around O1s changed and a new binding energy peak was generated. The peak separation of the O1s XPS patterns are shown in Fig. 6. The binding energies of O1s in the diatomite samples were 531.75 and 532.01 eV, which correspond to the binding energies of O-Si and O-H [12]. The binding energies of O1s in the Mn-diatomite samples were 529.33, 531.42, and 531.88 eV, which

correspond to the binding energies of O-Mn, O-Si, and O-H, respectively. Therefore, Mn bound to the diatomite surface in the modification process.

The Si2p XPS patterns of diatomite (D) and Mn-diatomite (Mn-D) are shown in Fig. 7. The Si2p binding energy of

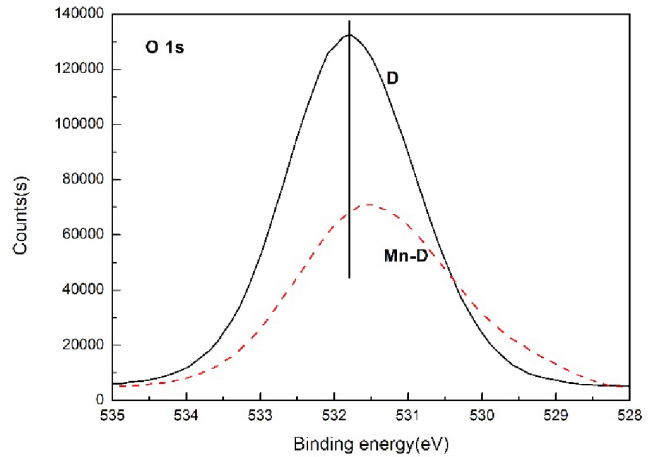


Fig. 5. O1s XPS patterns of diatomite and Mn-diatomite.

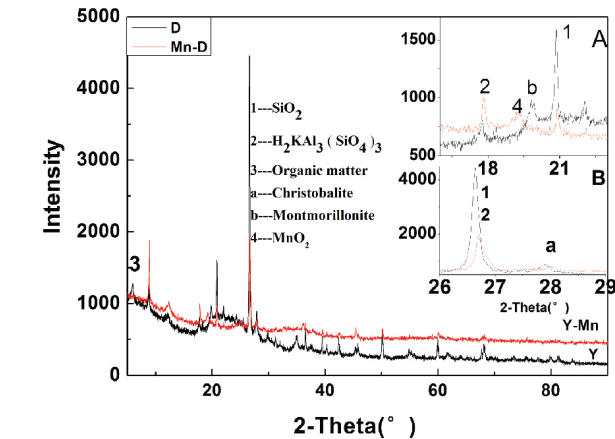
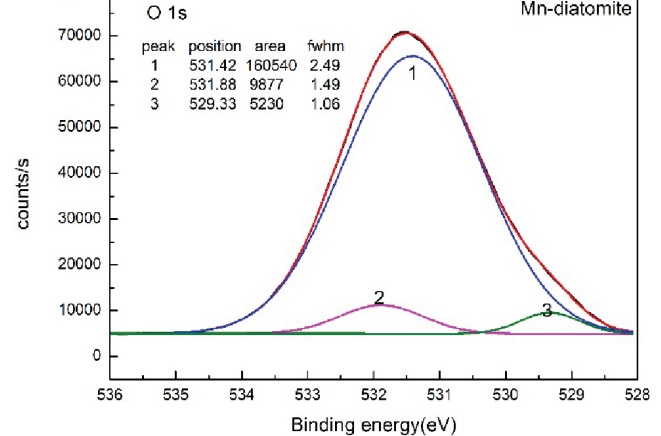
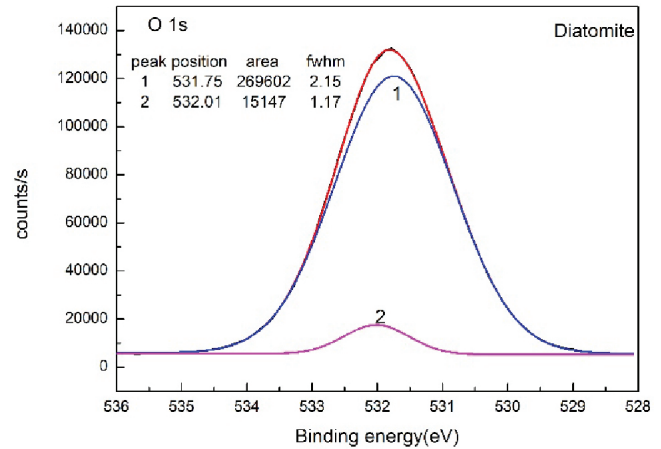


Fig. 4. XRD patterns for the diatomite (D) and Mn-diatomite (Mn-D).

Fig. 6. O1s XPS peak separations of diatomite and Mn-diatomite.

Mn-diatomite was lower than that diatomite, decreasing from 102.60 to 102.24 eV, and the electron cloud density in the vicinity of Si2p increased in the Mn-diatomite sample. There were several reasons for the binding energy reduction: impurities in the sample; some Si on the surface SiO₄ tetrahedrals were replaced by cations; the active hydroxyl groups on the surface were grafted by the modifier; and when part of the silane chain opened, the original –Si–O–Si– also opened, and some –Si–O–Mn– was generated. Therefore, the electron cloud density of O increased and the electro negativity decreased, leading to a lower Si2p binding energy.

As shown in Fig. 8, the main Mn2P binding energy peak of Mn-diatomite was asymmetric, therefore, the Mn in the sample was present in more than one chemical state. The valence state of Mn in the modifier was +2, and thus the Mn valence state changed in the modification process. The total binding energy of Mn on the Mn-diatomite surface increased beyond that of Mn²⁺, and the electron cloud density around Mn showed a decreasing trend [13].

The Mn2P XPS peak separation of Mn-diatomite is shown in Fig. 9. The binding energy of the Mn2P peak

could be divided into 640.32, 641.53, and 645.23 eV, which correspond to the binding energies of Mn²⁺, Mn³⁺, and Mn⁴⁺ oxides. This result indicated that the Mn oxidized, and its valence state changed during the modification. In the oxidation process, Mn with different valence states grafted to the diatomite surface.

The Pb4f XPS pattern of Mn-diatomite after adsorption is shown in Fig. 10. The binding energies of 138.13 and 143.05 eV correspond to Pb4f, which indicated a change compared with the binding energies of Pb4f before adsorption (138.3 and 141.7 eV). This result indicated that the Mn-diatomite adsorbed Pb(II).

The O1s, Si2p, and Mn2p XPS patterns of Mn-diatomite before and after Pb(II) adsorption are shown in Fig. 11. The O1s and Mn2p binding energy of Mn-diatomite after adsorption increased compared with the sample before adsorption, and after adsorption, the sample showed a tendency to lose electrons. The Si2p binding energy changed slightly; therefore, electrons may have shifted from Mn and O to Pb. The Pb(II) was absorbed around Mn and O.

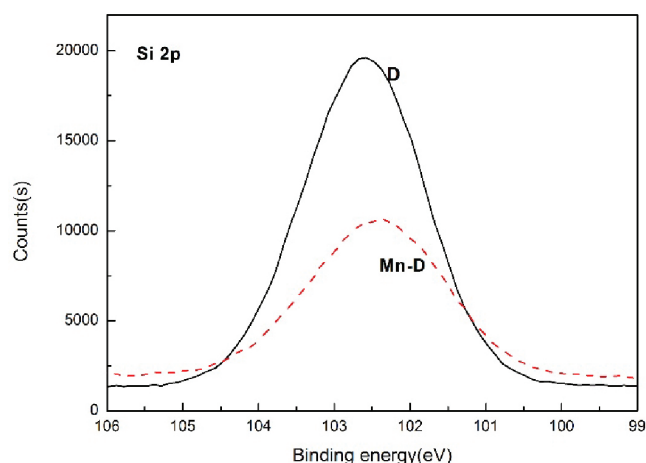


Fig. 7. Si2p XPS patterns of diatomite and Mn-diatomite.

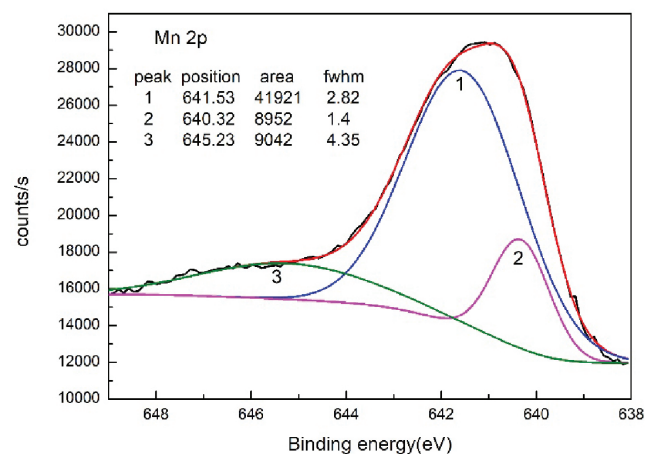


Fig. 9. Mn2p XPS peak separation pattern of Mn-diatomite.

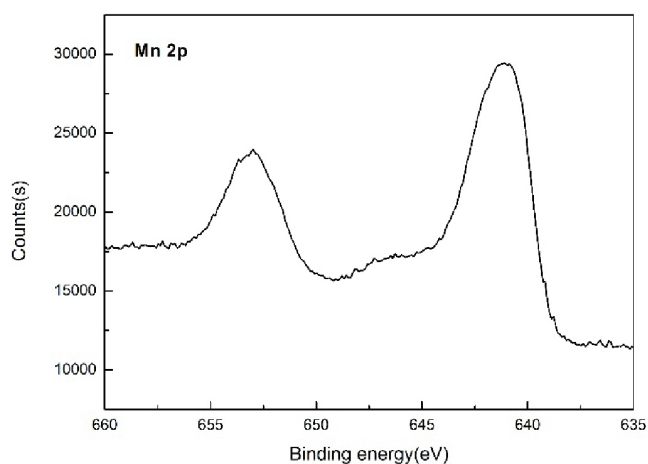


Fig. 8. Mn 2p XPS pattern of Mn-diatomite.

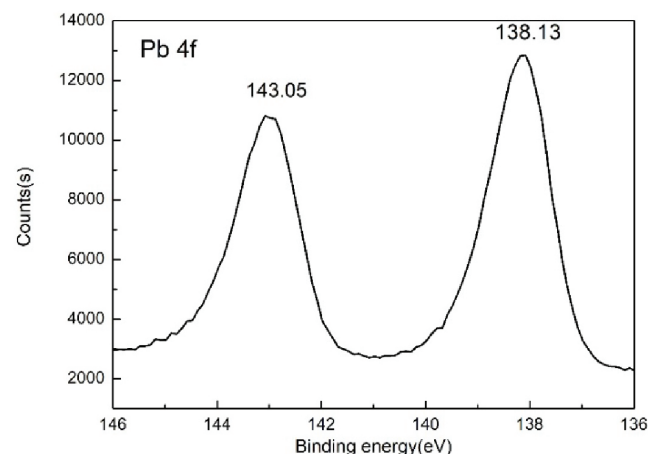


Fig. 10. Pb4f XPS pattern of Mn-diatomite after Pb(II) adsorption.

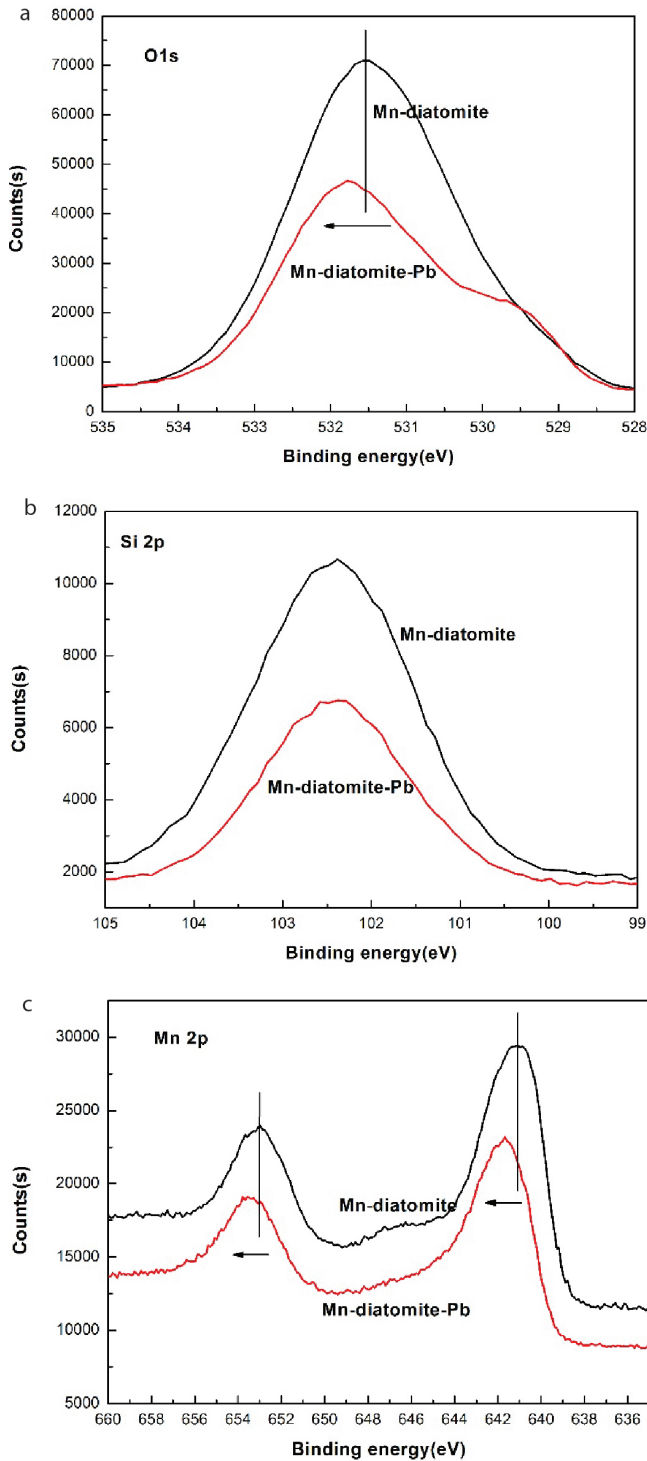


Fig. 11. O1s, Si2p, and Mn2p XPS patterns of Mn-diatomite before (Mn-diatomite) and after Pb(II) adsorption (Mn-diatomite-Pb).

3.1.6. Modification and adsorption mechanism analysis

Combined analysis of the XRD, SEM, FTIR, and XPS results revealed the modification mechanism. As shown in Fig. 12, several grafting processes occurred during the Mn

modification. There were abundant hydroxyl groups on the diatomite surface, and some of the active hydroxyl positions on the surface were replaced during Mn modification, as the Mn grafted to the diatomite surface. The Mn valence state changed in the modification process, resulting in several grafting methods (① in Fig. 12). Some siloxane bonds opened, forming more active surfaces with dangling bonds (② in Fig. 12). These ≡Si-O- or ≡Si- bonds combined easily with H⁺ and OH⁻ in aqueous solution and formed more active hydroxyl bonds at the surface, which benefited Mn grafting during modification. Some Si on the diatomite surface was also replaced by Mn during modification (③ in Fig. 12). In Fig. 12, the red underline marks show the positions where grafting could occur easily. These several Mn grafting mechanisms promoted the adsorption of Pb(II) around Mn and O.

3.2. Adsorption analysis

3.2.1. Effect of Mn-diatomite dose

The effect of Mn-diatomite on the adsorption of Pb(II) was examined under the following conditions: doses ranging from 0.1 g/L to 5 g/L, with an initial Pb solution concentration of 100 mg/L, pH of 5, and temperature of 25°C. The experiments were performed to establish appropriate adsorbent conditions for Pb(II) removal. As shown in Fig. 13, the Pb(II) removal increased from 24.3% to 99.8% when the Mn-diatomite dose increased from 0.1 to 5 g/L. This increase was attributed to the increased interference between the binding sites at higher doses or the insufficiency of metal ions in solution with respect to available binding sites. The removal rate increased rapidly when the dose of Mn-diatomite from 0.1 to 1 g/L. Increasing doses of diatomite increase the external diffusion parameter, a behavior that can be explained by the dependence of the external mass transfer coefficient on the driving force per unit area [14]. A similar behavior was observed when the dose of Mn-diatomite was increased to 1 g/L. Because resistance induced by intra particle diffusion is negligible when highly adsorbent masses are used, the 1 g/L Mn-diatomite dose was selected as the optimum adsorbent for further experiments.

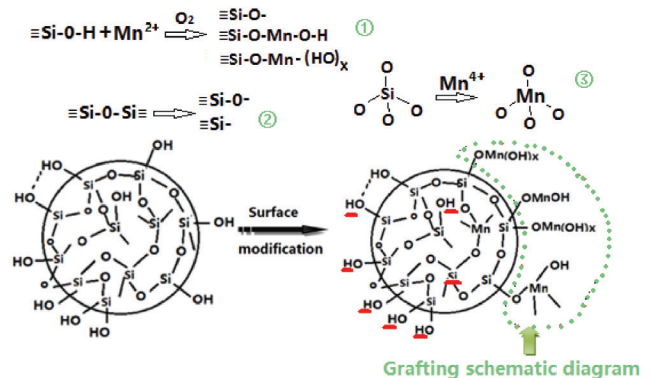


Fig. 12. Schematic of modification mechanism diagram; the red underline marks are the positions where graft substitution may occur.

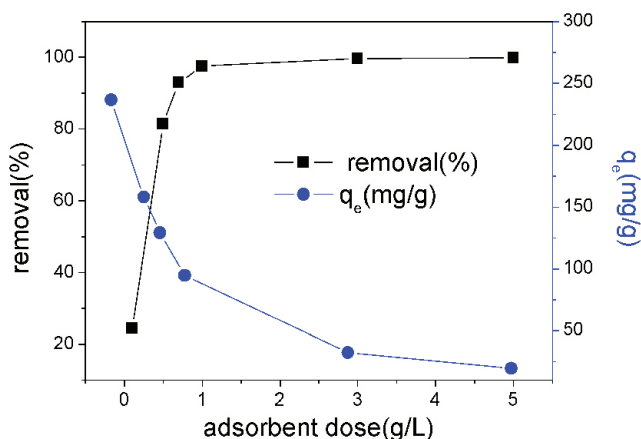


Fig. 13. Effect of adsorbent dose on Pb(II) removal.

3.2.2. Effect of initial solution pH

The pH of the adsorbent solutions is one of the major important factors affecting adsorption [15,16]. Fig. 14 illustrates the effect of pH on the Pb adsorption by Mn-diatomite in the pH range from 2.5 to 5 at 25°C for the initial Pb solution concentration of 100 mg/L. As shown, the Mn-diatomite adsorption significantly changed over this pH range. The adsorption capacity for Pb(II) increased as the pH increased up to 5. The zero point of charge (pHpzc) of the diatomite was 2.04. With SiO_2 as the active center of adsorption, the surface charge of Mn-diatomite was $-40 \mu\text{C cm}^{-1}$ [5]. The surface charge of MnO_2 was higher than those of other oxides, such as SiO_2 , TiO_2 , Al_2O_3 , and FeOOH , because of the former's high acidity constant. The surface of MnO_2 was ionized at low pH values and was charged more negatively compared with other oxides. The diatomite surface was charged negatively when the solution pH exceeded the pHpzc and was charged positively when the pH was below the pHpzc [7].

The maximum adsorption capacity increased from 43.9 to 92.7 mg/g with the increase in solution pH from 2.5 to 5. The metal uptake increased rapidly when the pH

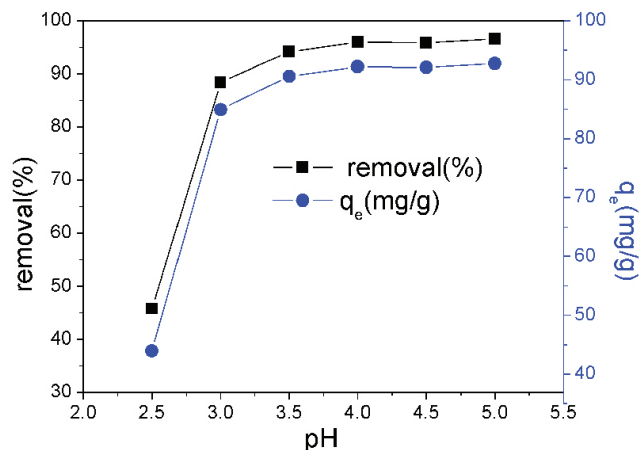


Fig. 14. Effect of pH on the Pb sorption onto the Mn-diatomite.

increased from 2.5 up to 4 and then increased slowly when the pH exceeded 4. Excessive protonation of the lone pair of electrons on N occurs at low pH values, which decreases the sorption of heavy metal ions [17]. At a very low solution pH, the concentration of H^+ also increases, resulting in changes in the ionic forms of the functional groups on the silica surface and competition between H^+ and metal ions [17,18] for active binding sites. The removal efficiency of Pb(II) increased from 94.1% to 96.6% when the pH increased from 3.5 to 5. The increase in the metal removal rate with increased pH can be attributed to decreasing H^+ in competition with positively charged metal ions at the adsorbent surface sites. Consequently, the solution pH of 5 was selected as an optimum value for further experiments.

3.2.3. Effect of initial Pb(II) concentration

Pb(II) adsorption by Mn-diatomite was examined at different initial Pb(II) concentrations (75, 100, 150, 200, 300, and 500 mg/L), with a pH of 5, Mn-diatomite dose of 1 g/L, and temperature of 25°C. The effects of the initial solution concentration on the adsorption of Pb(II) ions onto Mn-diatomite are shown in Fig. 15. As indicated in the figure, the adsorption of Pb(II) onto Mn-diatomite increased as the initial Pb(II) concentration increased. The removal rates of Pb(II) at equilibrium were 98.6%, 97.3%, 91.2%, 81.4%, 59.1%, and 36.4% at the initial concentrations of 75, 100, 150, 200, 300, and 500 mg/L, respectively. Fig. 15 shows that the adsorption capacity of Mn-diatomite for Pb(II) ion increased linearly with the increasing initial concentration of Pb(II). High initial Pb(II) concentrations enhance the adsorption [7]. Therefore, the initial Pb(II) concentration of 200 mg/L was selected as the optimum concentration for further experiments.

3.2.4. Adsorption isotherms

The adsorption of Pb(II) onto Mn-diatomite was examined under the following conditions: varying initial Pb(II) concentrations (75, 100, 150, 200, 300, and 500 mg/L), pH of 5, Mn-diatomite dose of 1 g/L, and temperature of

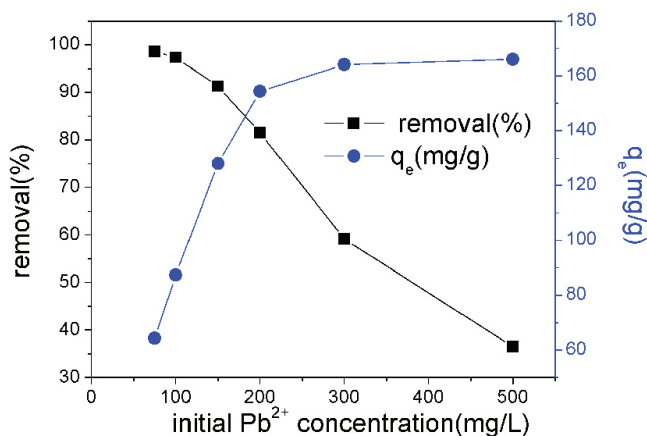


Fig. 15. Effect of initial concentration on Pb(II) removal.

25°C. The results were applied successively to the Langmuir and Freundlich adsorption models [19].

The Mn-diatomite adsorption isotherm curve at different temperatures exhibits an “L” form [20]. Fig. 16 shows that the adsorption of Pb(II) on Mn-diatomite increased with increasing initial Pb(II) concentrations. Further increases in temperature lead to increased adsorption of Pb(II), indicating that the adsorption process is endothermic.

The experimental data were applied successively to the Langmuir and Freundlich adsorption models by the equations $\frac{C_e}{q_e} = \frac{1}{bQ} + \frac{C_e}{Q}$ and $\log q_e = \log K_F + \frac{1}{n} \log C_e$ [19],

where Q is the mono layer capacity (mg/g), b is the equilibrium constant (L/mg), and K_F (mg/g) and n are the Freundlich constants related to adsorption capacity and adsorption intensity, respectively.

The separation factor could be obtained from the

following relation: $R_L = \frac{1}{1 + bC_o}$, where $0 < R_L < 1$ indicates

favorable adsorption, $R_L > 1$ indicates unfavorable adsorption, $R_L = 1$ indicates linear adsorption, and $R_L = 0$ indicates irreversible adsorption [21].

Fig. 17 shows the Langmuir plot of C_e versus C_e/q_e . The Freundlich plot of $\log C_e$ versus $\log q_e$ is shown in Fig. 18. The parameters of all adsorption isotherm models of Pb(II) for Mn-diatomite at three working temperatures are listed in Table 2.

Table 2 shows that compared with the Freundlich isotherm, the Langmuir isotherm provided a better correlation with the experimental data for the adsorption of Pb(II) ion onto Mn-diatomite. The Langmuir mono layer adsorption capacity Q was large, with values between 138.9 and 166.7 mg/g for Mn-diatomite. The dimensionless separation factors R_L were 0.0256, 0.0292, and 0.0327 for Mn-diatomite at 25, 35, and 45°C, respectively. The R_L values showed that Mn-diatomite was favorable for the sorption of Pb(II) ion.

The n adsorption levels determined from the Freundlich adsorption isotherm were 6.109, 6.285, and 7.508 for Mn-diatomite at 25, 35, and 45°C, respectively. $n = 1$ indicates

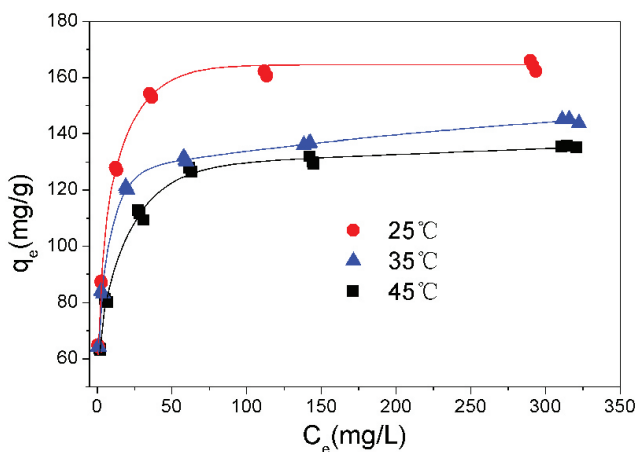


Fig. 16. Adsorption isotherms of Pb(II) on Mn-diatomite.

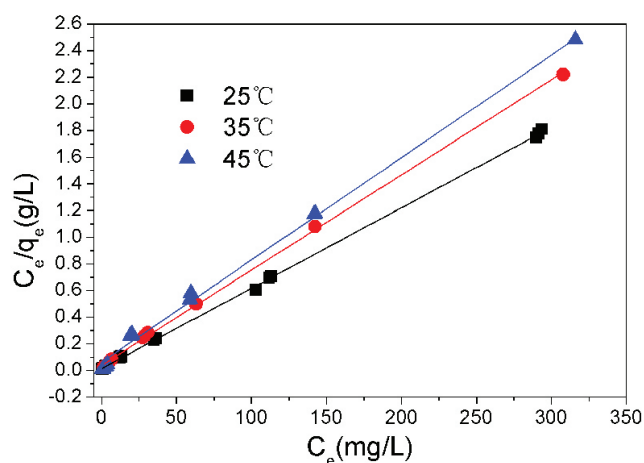


Fig. 17. Langmuir model of adsorption isotherm of Pb(II) on Mn-diatomite.

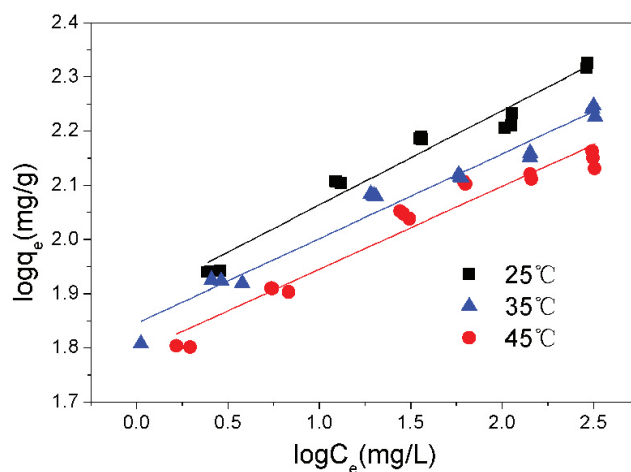


Fig. 18. Freundlich model of adsorption isotherm of Pb(II) on Mn-diatomite.

linear adsorption and equal adsorption energies for all sites. Values of n between 1 and 10 indicate good adsorption [22], whereas $n < 1$ indicates decreased marginal adsorption energy with increasing surface concentration [23]. The calculated n values indicated that the adsorption processes were favorable.

3.2.5. Adsorption kinetics

Adsorption kinetics show the rate of adsorption on an adsorbent and determines the equilibrium time. The effect of reaction time on the adsorption of Pb(II) onto the Mn-diatomite samples is shown in Fig. 19. The measurements were obtained over a period of 2 to 120 min. In all cases, a contact time of 30 min was sufficient to ensure adsorption equilibrium. Rapid removal of Pb(II) by adsorption on Mn-diatomite was observed during the initial period of contact before 25 min. As contact time increased, the removal became slower and more stagnant.

Table 2
Parameters of Langmuir and Freundlich equations for Mn-diatomite

Temperature (°C)	Langmuir			Freundlich			
	Q (mg/g)	B (L/g)	R_L	R_2	K_F (mg/g)	n	R_2
25°C	166.7	0.438	0.0256	0.9996	75.4	6.109	0.9515
35°C	140.8	0.383	0.0292	0.9993	71.1	6.285	0.9154
45°C	138.9	0.341	0.0327	0.9902	60.6	7.508	0.9151

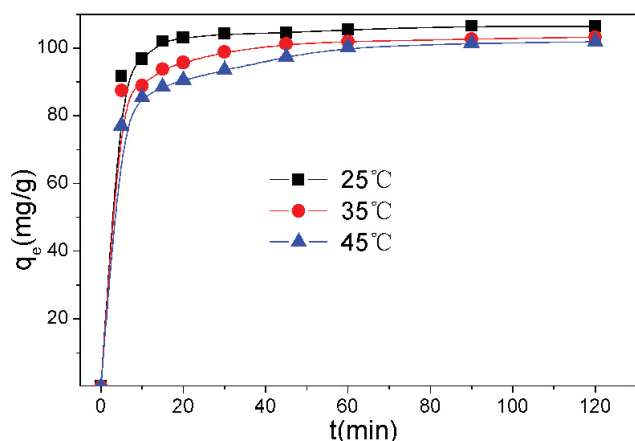


Fig. 19. Effect of reaction time on Pb(II) adsorption onto Mn-diatomite.

Pb(II) was transported rapidly to the external surface of the Mn-diatomite particles by film diffusion because of the higher concentration gradient during the initial period [24], resulting in a higher adsorption rate. The slow adsorption rate during the late stage was attributed to the slow diffusion of solute into the interior of the adsorbent [25].

The experimental data were fitted to pseudo-first-order and pseudo-second-order models for Mn-diatomite

according to $\ln(q_e - q) = \ln q_e - K_1 t$ and $\frac{t}{q} = \frac{1}{k_2 q_e^2} + \frac{t}{q_e}$,

respectively, where k_1 is the pseudo-first-order rate constant (min^{-1}), and k_2 is the pseudo-second-order rate constant ($\text{g}/(\text{mg}\cdot\text{min})$). Initial Pb(II) concentrations of 100 mg/L at 25, 35, and 45°C were used in the calculations. The linear plot of $\ln(q_e - q)$ against t according to the pseudo-first-order model is shown in Fig. 20. k_1 and q_e can be derived from the slope and the intercept of the plot. Fig. 21 shows the variation of t/q_1 against t according to the pseudo-second-order model. The rate constants q_e and k_2 can be derived from the slope and the intercept. The kinetic parameters for all experimental data as determined by the pseudo-first-order and pseudo-second-order models are listed in Table 3.

Table 3 shows that the q_e values calculated from the pseudo-first-order model do not match the q_e experimental results. The R_2 values ranged from 0.8304 to 0.9344. Similarities between the q_e values obtained by experiments and calculation were observed from the pseudo-second-order model, where the R_2 values ranged from 0.9991 and 0.9998. The mechanism of Pb(II) adsorption onto Mn-diatomite can be explained by pseudo-second-order reaction kinetics. Consequently, all

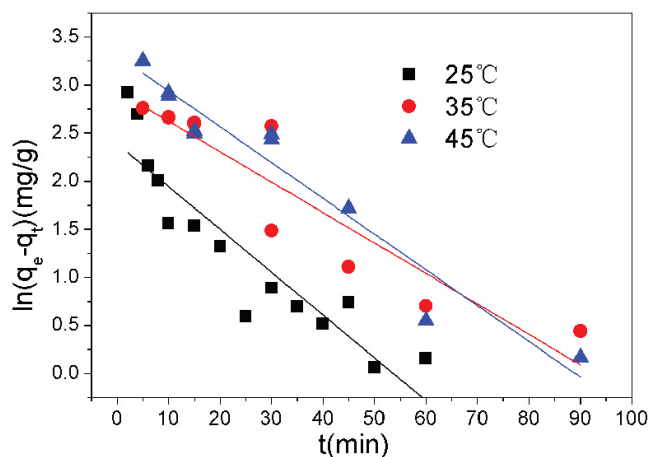


Fig. 20. Pseudo-first-order adsorption kinetics of Pb(II) onto Mn-diatomite.

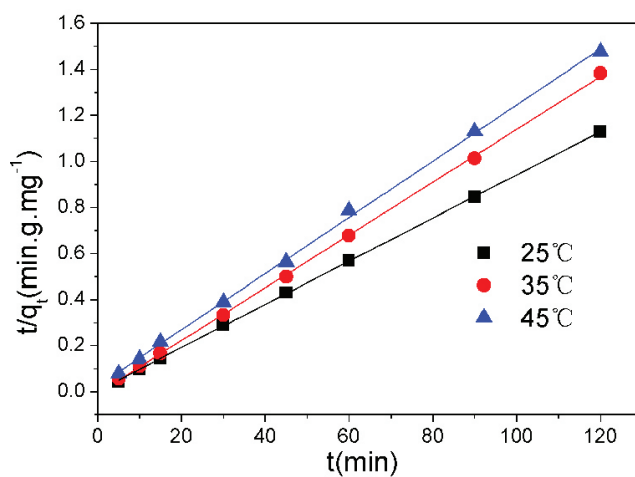


Fig. 21. Pseudo-second-order adsorption kinetics of Pb(II) onto Mn-diatomite.

kinetic data from this study were analyzed using this model to estimate the adsorption capacity, rate constant, and initial adsorption rate obtained from Mn-diatomite.

3.2.6. Analysis of adsorption thermodynamics

Thermodynamic parameters provide additional detail regarding the inherent energetic changes that occur during

Table 3
Parameters of pseudo-first-order and pseudo-second-order kinetic models for Mn-diatomite

Temperature (°C)	Pseudo-first-order kinetic model			Pseudo-second-order kinetic model		
	q_e (mg/g)	k_1 ($\times 10^{-3} \text{ min}^{-1}$)	R_2	q_e (mg/g)	k_2 ($\times 10^{-3} \text{ g} \cdot \text{mg}^{-1} \cdot \text{min}^{-1}$)	R_2
25°C	22.284	84.82	0.8304	96.862	47.63	0.9996
35°C	32.871	83.34	0.8606	90.580	60.03	0.9991
45°C	25.071	42.13	0.9344	81.673	8.33	0.9998

adsorption [26]. The important thermodynamic parameters are the standard enthalpy change (ΔH°), the standard entropy change (ΔS°), and the Gibbs free energy change (ΔG°), which are calculated using equations (3), (4), and (5), respectively:

$$K_d = \frac{q_e}{C_e} \quad (3)$$

$$\ln K_d = \frac{\Delta S^\circ}{R} - \frac{\Delta H^\circ}{RT} \quad (4)$$

$$\Delta G^\circ = \Delta H^\circ - T\Delta S^\circ \quad (5)$$

Here, K_d is the thermodynamic equilibrium constant (mL/g), T is the temperature (K), and R is the gas constant (8.314 J/(mol·K)). The thermodynamic parameters obtained from the above equations are listed in Table 4.

The results clearly show the spontaneous and thermodynamically favorable adsorption of Pb(II), based on the negative value of the Gibbs free energy change (ΔG°) [27]. With increasing initial concentration and temperature, the value of ΔG° increases, which indicates that the adsorption effect is better at lower initial concentrations and temperatures [28]. The negative value of ΔH° confirms the exothermic nature of sorption, and the absolute value of ΔH° , less than 40 kJ/mol, indicates that the mechanism of adsorption is physical adsorption. The negative values of ΔS° indicate the decreasing randomness at the adsorbent-adsorbate interface during the adsorption [28].

3.2.7. Reusability

Ten cycles of adsorption–desorption of Pb(II) onto the Mn-diatomite were performed at an initial Pb concentration of 200 mg L⁻¹ and 25°C. The results are shown in Fig. 22.

The desorption of Pb(II) from Mn-diatomite was achieved by treatment with 0.5 M HCl. The desorption time was fixed at 40 min for each cycle. The adsorption

Table 4
Thermodynamic parameters for Pb(II) adsorption onto Mn-diatomite

C_0 (mg/L)	ΔH° (kJ/mol)	ΔS° J/(mol·K)	ΔG° (kJ/mol)		
			298 K	308 K	318 K
150	-38.66	-52.93	-22.89	-22.36	-21.83
200	-29.58	-30.55	-20.47	-20.17	-19.86
300	-18.83	-2.82	-17.99	-17.96	-17.94

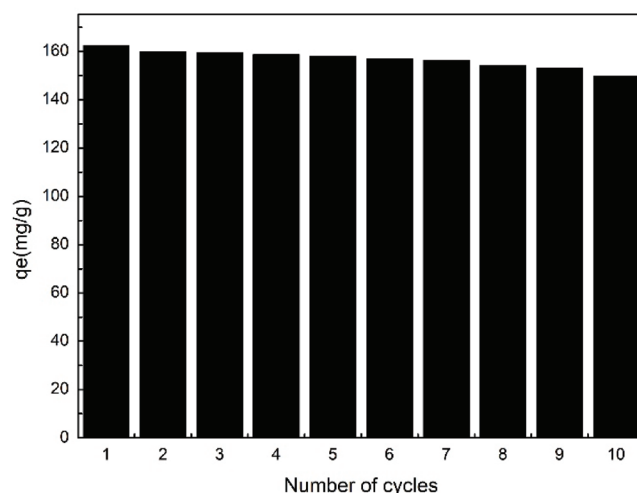


Fig. 22. Ten cycles of Pb adsorption–desorption with 0.5 M HCl.

capacity of Pb(II) onto the Mn-diatomite decreased from 162.3 mg g⁻¹ in the first cycle to 149.7 mg/g in the tenth cycle. This showed that the Mn-diatomite could be reused with very little loss in the adsorption performance.

3.2.8. Comparison of Mn-diatomite with other adsorbents

Table 5 compares the maximum adsorption capacity of Mn-diatomite with other adsorbents reported in the literature. The maximum adsorption capacity of Pb(II) onto the Mn-diatomite was higher than those of all of these previously reported adsorbents; therefore, Mn-diatomite has significant potential for adsorption of Pb(II) from aqueous systems.

3.2.9. Treatment of electrolytic Zn rinse wastewater

Zn electrolysis production produces lots of rinse wastewater that contains Zn, Pb, Cd, As, and other heavy metal ions; the emission of this wastewater is harmful to the environment and to public health. The electrolytic Zn rinse wastewater used in this experiment was collected from Guangxi Jinshan Indium and Germanium Metallurgical Chemical Co., Ltd. The main constituents are shown in Table 6.

The effect of Mn-diatomite on the adsorption of real wastewater was examined under the following conditions: adsorbent dosage of 5 g/L, pH of 5.46, time of 90 min, and temperature of 25°C. The removal rates of Pb(II), Cd(II), and Zn(II) were 98.84%, 54.75%, and 28.70%, respectively.

Table 5
Pb(II) sorption capacities (mg/g) for Mn-diatomite and other adsorbents in the literature

Adsorbent	Adsorption capacity of Pb(II) (mg/g)	References
Nano-scale zero valent iron (nZVI)	50.31	[29]
Magnetic biochar (MBC)	27	[30]
Manganoxide minerals	98	[31]
Carbon nanotube sheet	117.64	[32]
Mesoporous activated carbon	20.3	[33]
PAC A	112	[34]
Acid-B-SBA-K	135.54	[35]
Mn-diatomite	166.7	This study

Table 6
Main constituents of electrolytic Zn rinse wastewater (mg/L)

Zn	483.62
Cu	0.73
Cd	7.59
Pb	2.60
As	2.00
pH	5.46

The concentrations of Pb(II), Cu(II), and As(V) after adsorption were 0.03, 0.01, and 0.09 mg/L, which satisfy the requirements of Pb and Zn Industrial Pollutant Discharge Standards (GB25466-2010).

4. Conclusions

The characterizations of diatomite and Mn-diatomite demonstrated that MnO₂ had been successfully grafted onto the surface of diatomite after modification. The modification also produced an eight-fold increase in the adsorbent's specific surface area. The Pb sorption capacity of diatomite was improved after modification. This improvement in diatomite performance was attributed to increased surface area, as well as the grafted MnO₂ on the diatomite surface.

The adsorbent dose, pH, and initial Pb concentration effected the sorption capacity. The removal rate of Pb(II) increased with increasing adsorbent doses from 0.1 to 5 g/L. However, the adsorption capacity exhibited the opposite behavior. The removal rate of Pb(II) increased with increasing pH from 2.5 to 5. Thus, the solution pH of 5 and adsorbent dose of 1 g/L were selected as optimum values for further experiments. The adsorption capacities of Pb(II) increased with increasing initial Pb(II) concentrations.

The removal processes followed the Langmuir isotherm model and pseudo-second-order kinetics model. The adsorption process was spontaneous and endothermic. The

present study showed that Mn-diatomite can be used as a readily available adsorbent for Pb removal from aqueous solution.

Acknowledgment

This work was supported by the National Natural Science Foundation of China (No. 41662005), Guangxi Science and Technology Project (No. 14124004-5-5), the Project of High Level Innovation Team and Outstanding Scholar in Guangxi Colleges and Universities (No. 002401013001), and Guangxi Scientific Experiment Center of Mining, Metallurgy, and Environment (No. KH2012ZD004).

References

- [1] Q. Li, J. Zhai, W. Zhang, M. Wang, J. Zhou, Kinetic studies of adsorption of Pb(II), Cr(III) and Cu(II) from aqueous solution by sawdust and modified peanut husk, *J. Hazard. Mater.*, 141 (2007) 163–167.
- [2] H. Beheshti, M. Irani, Removal of lead(II) ions from aqueous solutions using diatomite nano particles, *Desa. Water Treat.*, 57 (2015) 18799–18805.
- [3] M. Irani, M. Amjadi, M.A. Mousavian, Comparative study of lead sorption onto natural perlite, dolomite and diatomite, *Chem. Eng. J.*, 178 (2011) 317–323.
- [4] Y.-B. Shen, Y.M. Zhu, Z.A. Wang, D.Z. Wei, Adsorption of Pb²⁺ in hydrofacies by diatomite, *J. Northeast. U. Nat. Sci.*, 24 (2003) 982–985.
- [5] Y. Al-Degs, M. Khraisheh, M. Tutunji, Sorption of lead ions on diatomite and manganese oxides modified diatomite, *Water Res.*, 35 (2001) 3724–3728.
- [6] M. Al-Ghouti, Development of a flow injection method for studying adsorption processes, and to investigate its use in the removal of some water pollutants, Master's Thesis, University of Jordan, Amman, Jordan, (1999).
- [7] M.A. Al-Ghouti, Y.S. Al-Degs, M.A. Khraisheh, M.N. Ahmad, S.J. Allen, Mechanisms and chemistry of dye adsorption on manganese oxides-modified diatomite, *J. Environ. Manag.*, 90 (2009) 3520–3527.
- [8] J. Luo, Q. Zhang, S.L. Suib, Mechanistic and kinetic studies of crystallization of birnessite, *Inorg. Chem.*, 39 (2000) 741–747.
- [9] B. Yilmaz, N. Ediz, The use of raw and calcined diatomite in cement production, *Cem. Concr. Compos.*, 30 (2008) 202–211.
- [10] Y. Jiang, Q. Gao, H. Yu, Y. Chen, F. Deng, Intensively competitive adsorption for heavy metal ions by PAMAM-SBA-15 and EDTA-PAMAM-SBA-15 inorganic-organic hybrid materials, *Micro porous Meso porous Mater.*, 103 (2007) 316–324.
- [11] M. Khraisheh, Y. Aldegs, W. McMinn, Remediation of wastewater containing heavy metals using raw and modified diatomite, *Chem. Eng. J.*, 99 (2004) 177–184.
- [12] G.P. López, D.G. Castner, B.D. Ratner, XPS O 1s binding energies for polymers containing hydroxyl, ether, ketone and ester groups, *Surf. Interface Anal.*, 17 (2010) 267–272.
- [13] J. Wu, H. Zheng, J.F. Mitchell, C. Leighton, Colossal magneto transport phenomena due to phase competition in Pr 1– x (Ca y Sr 1– y) x MnO₃ single crystals, *J. Magn. Magn. Mater.*, 288 (2005) 146–154.
- [14] M.A. Al-Ghouti, M.A. Khraisheh, M.N. Ahmad, S. Allen, Adsorption behaviour of methylene blue onto Jordanian diatomite: a kinetic study, *J. Hazard. Mater.*, 165 (2009) 589–598.
- [15] C. Chen, X. Wang, Sorption of Th (IV) to silica as a function of pH, humic/fulvic acid, ionic strength, electrolyte type, *Appl. Radiat. Isot.*, 65 (2007) 155–163.
- [16] A. Sari, D. Mendil, M. Tuzen, M. Soylak, Biosorption of Cd(II) and Cr(III) from aqueous solution by moss (*Hylacomium splendens*) biomass: equilibrium, kinetic and thermodynamic studies, *Chem. Eng. J.*, 144 (2008) 1–9.

- [17] A. Benhamou, M. Baudu, Z. Derriche, J.P. Basly, Aqueous heavy metals removal on amine-functionalized Si-MCM-41 and Si-MCM-48, *J. Hazard. Mater.*, 171 (2009) 1001–1008.
- [18] A. Heidari, H. Younesi, Z. Mehraban, Removal of Ni (II), Cd (II), and Pb (II) from a ternary aqueous solution by amino functionalized mesoporous and nano mesoporous silica, *Chem. Eng. J.*, 153 (2009) 70–79.
- [19] R. Liu, Y. Lu, X. Shen, Q. Liang, Q. Wang, Arsenic (V) adsorption from aqueous solution on magnetic Fe₀. 2 (Co₂₀Ni₈₀) 0.8 alloy porous microfibers, *Water Air Soil Pollut.*, 223 (2012) 5365–5373.
- [20] M. Safa, M. Larouci, B. Meddah, P. Valemens, The sorption of lead, cadmium, copper and zinc ions from aqueous solutions on a raw diatomite from Algeria, *Water Sci. Technol.*, 65 (2012) 1729–1737.
- [21] B. Hameed, J. Salman, A. Ahmad, Adsorption isotherm and kinetic modeling of 2, 4-D pesticide on activated carbon derived from date stones, *J. Hazard. Mater.*, 163 (2009) 121–126.
- [22] J.U.K. Oubagaranadin, Z. Murthy, Adsorption of divalent lead on a montmorillonite–illite type of clay, *Ind. Eng. Chem. Res.*, 48 (2009) 10627–10636.
- [23] H. Koyuncu, A.R. Kul, N. Yıldız, A. Çalımlı, H. Ceylan, Equilibrium and kinetic studies for the sorption of 3-methoxybenzaldehyde on activated kaolinites, *J. Hazard. Mater.*, 141 (2007) 128–139.
- [24] K.G. Bhattacharyya, A. Sharma, Kinetics and thermodynamics of methylene blue adsorption on neem (*Azadirachta indica*) leaf powder, *Dyes Pigments*, 65 (2005) 51–59.
- [25] M.Q. Jiang, Q.P. Wang, X.Y. Jin, Z.L. Chen, Removal of Pb (II) from aqueous solution using modified and unmodified kaolinite clay, *J. Hazard. Mater.*, 170 (2009) 332–339.
- [26] O. Moradi, K. Zare, M. Yari, Interaction of some heavy metal ions with single walled carbon nano tube, *Int. J. Nano Dimens.*, 1 (2011) 203–220.
- [27] F. Karkehabadi, S. Sabersamandari, S. Sabersamandari, The impact of functionalized CNT in the network of sodium alginate-based nano composite beads on the removal of Co(II) ions from aqueous solutions, *J. Hazard. Mater.*, 312 (2016) 224–233.
- [28] E. Unuabonah, K. Adebawale, B. Olu-Owolabi, Kinetic and thermodynamic studies of the adsorption of lead (II) ions onto phosphate-modified kaolinite clay, *J. Hazard. Mater.*, 144 (2007) 386–395.
- [29] N. Arancibia-Miranda, S.E. Baltazar, A. García, A.H. Romero, M.A. Rubio, D. Altbir, Lead removal by nano-scale zero valent iron: surface analysis and pH effect, *Mater. Res. Bull.*, 59 (2014) 341–348.
- [30] A.G. Karunanayake, O.A. Todd, M. Crowley, L. Ricchetti, C.U. Pittman, R. Anderson, D. Mohan, T. Mlsna, Lead and cadmium remediation using magnetized and non magnetized biochar from Douglas fir, *Chem. Eng. J.*, 331 (2018) 480–491.
- [31] A. Sönmezay, M.S. Öncel, N. Bektaş, Adsorption of lead and cadmium ions from aqueous solutions using manganoxide minerals, *Trans. Nonferrous Met. Soc. of China*, 22 (2012) 3131–3139.
- [32] M.A. Tofighy, T. Mohammadi, Adsorption of divalent heavy metal ions from water using carbon nano tube sheets, *J. Hazard. Mater.*, 185 (2011) 140–147.
- [33] E. Asuquo, A. Martin, P. Nzerem, F. Siperstein, X. Fan, Adsorption of Cd(II) and Pb(II) ions from aqueous solutions using mesoporous activated carbon adsorbent: equilibrium, kinetics and characterisation studies, *J. Environ. Chem. Eng.*, 5 (2017) 679–698.
- [34] L. Largette, T. Brudey, T. Tant, P.C. Dumesnil, P. Lodewyckx, Comparison of the adsorption of lead by activated carbons from three lignocellulosic precursors, *Micro porous Meso porous Mater.*, 219 (2016) 265–275.
- [35] H.C. Tao, H.R. Zhang, J.B. Li, W.Y. Ding, Biomass based activated carbon obtained from sludge and sugarcane bagasse for removing lead ion from wastewater, *Bioresour. Technol.*, 192 (2015) 611–617.